WILEY-VCH

Supporting Information

Additive manufacturing-enabled architected nanocomposite lattices coated with plasmonic nanoparticles for water pollutants detection

Sara Fateixa,[a] Marc Landauer,[b] Johannes Schneider,[c] Shanmugam Kumar,[c*] Robert Böhm[b]*

[a]: Department of Chemistry – CICECO Aveiro Institute of Materials, University of Aveiro, 3810-193, Aveiro, Portugal.

[b]: HTWK Leipzig, Faculty of Engineering, PF 30 11 66, 04251 Leipzig, Germany

[c]: James Watt School of Engineering, University of Glasgow, Glasgow, G12 8LT, UK

E-mail: msv.kumar@glasgow.ac.uk; sarafateixa@ua.pt

Table S1: Assignments of the bands on the Raman spectrum of neat PP filaments acquired with a 532nm laser.[1]

Raman band (cm^{-1})	Assignment
2956	$\upsilon_{asym}(CH_3)$
2896	$\upsilon(CH)$
2885	$\upsilon_{sym}(CH_3)$
2840	$\upsilon_{sym}(CH_2)$
1458	$\upsilon_{asym}(CH_3)$; $\delta(CH_2)$
1334	$\delta(CH)$, $\tau(CH_2)$
1218	$\tau(CH_2)$, $\delta(CH)$, $\upsilon(CC)$
1156	$\upsilon(CC)$, $\upsilon(C\text{-}CH_3)$, $\delta(CH)$, $\rho(CH_3)$
1036	$\upsilon(C\text{-}CH_3)$, $\upsilon(CC)$, $\delta(CH)$
998	$\rho(CH_3)$, $\delta(CH)$,$\varpi(CH_2)$
970	$\rho(CH_3)$, $\upsilon(CC)$,
846	$\rho(CH_2)$, $\upsilon(CC)$, $\upsilon(C\text{-}CH_3)$, $\rho(CH_3)$
808	$\rho(CH_2)$, $\upsilon(CC)$, $\upsilon(C\text{-}CH_3)$
534	$\varpi(CH_2)$, $\upsilon(C\text{-}CH_3)$, $\rho(CH_2)$
454	$\varpi(CH_2)$
405	$\varpi(CH_2)$, $\delta(CH)$

Table S2: Experimental Raman band positions (wavenumber, cm^{-1}) for methylene blue (MB)[2–4] thiram[5–7] and paraquat[8–10] with the corresponding vibrational mode assignments.

Wavenumber (cm^{-1})	**Vibrational modes**
MB	
1618	ν(CC) + δ(CH) in plane (ring), ν(CN) + ν(CC)
1485	ν_{sym}(CN) (lateral) + δ(CH) in plane (ring) + δ(CH) out of plane (CH_3), ν(CC)
1430	δ(CH) out of plane (CH_3), ν(CC), ν_{sym}(CN)
1392	ν_{sym}(CN) (lateral and centre) + δ(CH) in plane (ring) + δ(CH) out of plane (CH_3), ν(CN) + ν(CC), ν_{asym}(CN)
1181	δ(CH) in plane (ring) + δ(CH) out of plane (CH_3), δ(CH) in plane
770	Skeletal deformation (CN and CH_3), δ(CH) in plane
677	Skeletal deformation (CC), δ(CH) in plane
583	Torsion of molecule + δ(CH) out of plane (ring), CC skeletal deformation
494	Thiazine ring in-plane bending
441	Skeletal deformation (CN, CS and CH_3), CN skeletal deformation
Thiram	
1452	$\delta_{asym}(CH_3)$
1369	ν(C-N) coupled to δsym(CH_3)
1140	ρ(CH_3) and ν(C–N)
970 and 1035	ν(C-S) and ν(C=S)
845	–CH_3 groups (several vibrational modes)
554	ν_{sym}(CSS) coupled to ν(S-S)
437	δ(CSS) and δ(CNC)
389	ν(S-S)
356	ν(CH_3-NC)
Paraquat	
1642	ν(C=N)
1293	(C-C) structural distortion
1191	δ(C=C)
837	ν(C-N)

Table S3: BET surface area, total porosity and average pore diameter of 3D scaffold samples

Sample	**SBET (m^2/g)[1]**	**V_T (cm^3/g)[2]**	**D_P (nm)[3]**
3D_PPcel	2.48	0.0295	5.79
3D_PP4%cell	0.73	0.0095	5.78
3D_Ag/PP4%cell	13.91	0.0137	5.79
3D_Ag/PP4%non	3.12	0.0102	3.11

[1]: specific surface area; [2]: total porosity; [3]: average pore diameter

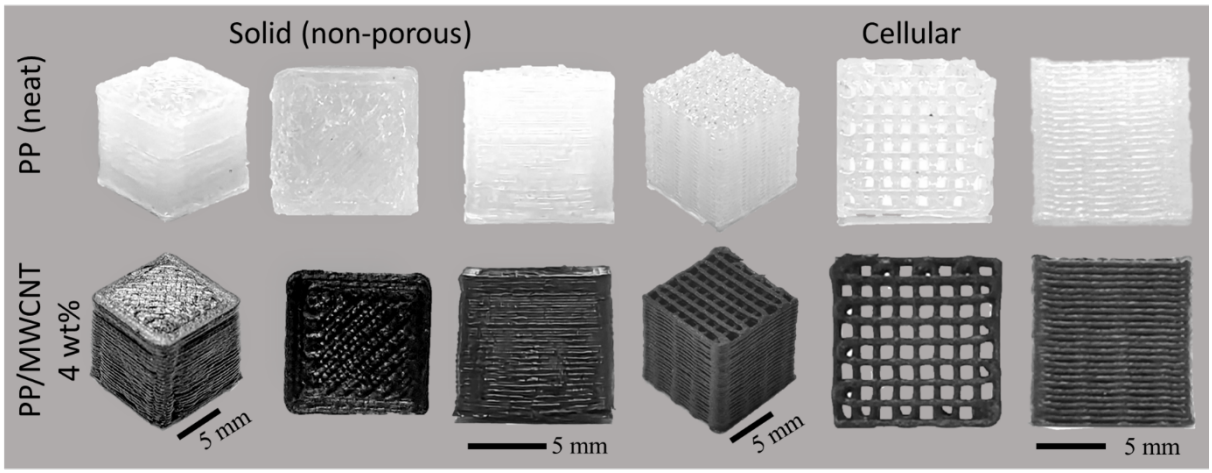

Figure S1: Solid (non-porous) and cellular architectures printed via FFF using PP (neat) and PP/MWCNT 4wt%.

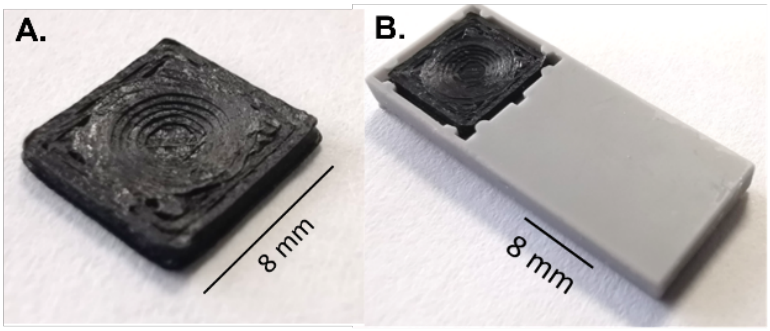

Figure S2: A) the test stripe insert; B) the test stripe base plate.

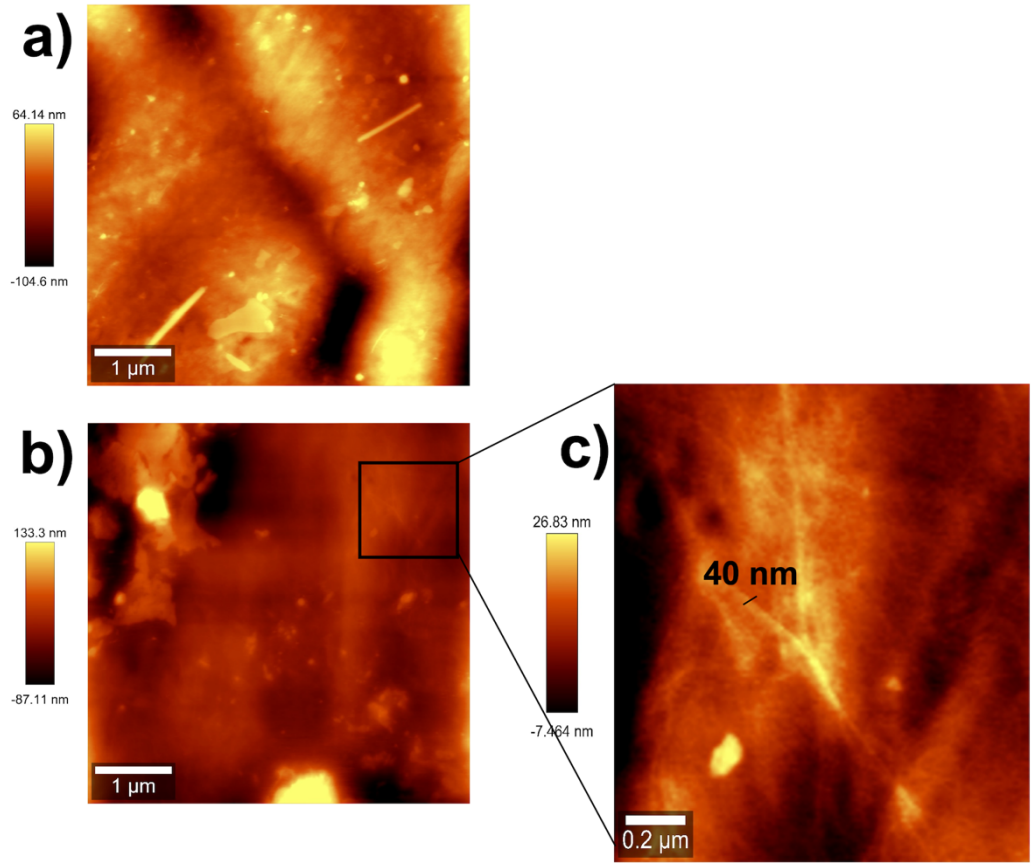

Figure S3: AFM topography images of PP (a) and PP4% (b) filaments. High-resolution AFM topography image of MWCNTs at the surface of the PP4% filament (c).

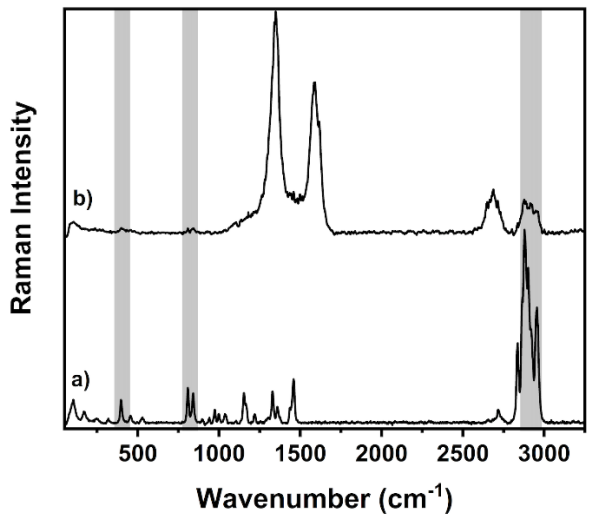

Figure S4: Average of 5 Raman spectra of neat PP (a) and PP4% (b) filaments (532nm laser source; 1mW, 5s, 10acquisitions).

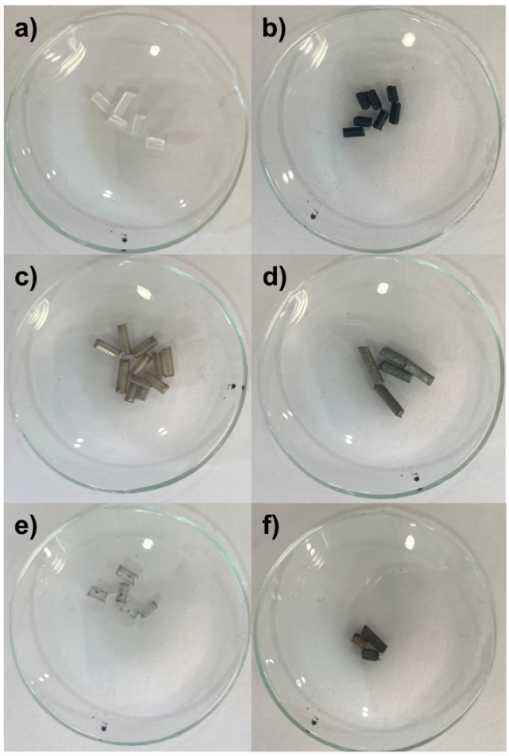

Figure S5: Digital photographs of PP (a), PP4% (b); Ag/PP (c), Ag/PP4% (d), Au/PP (e), Au/PP4% (F).

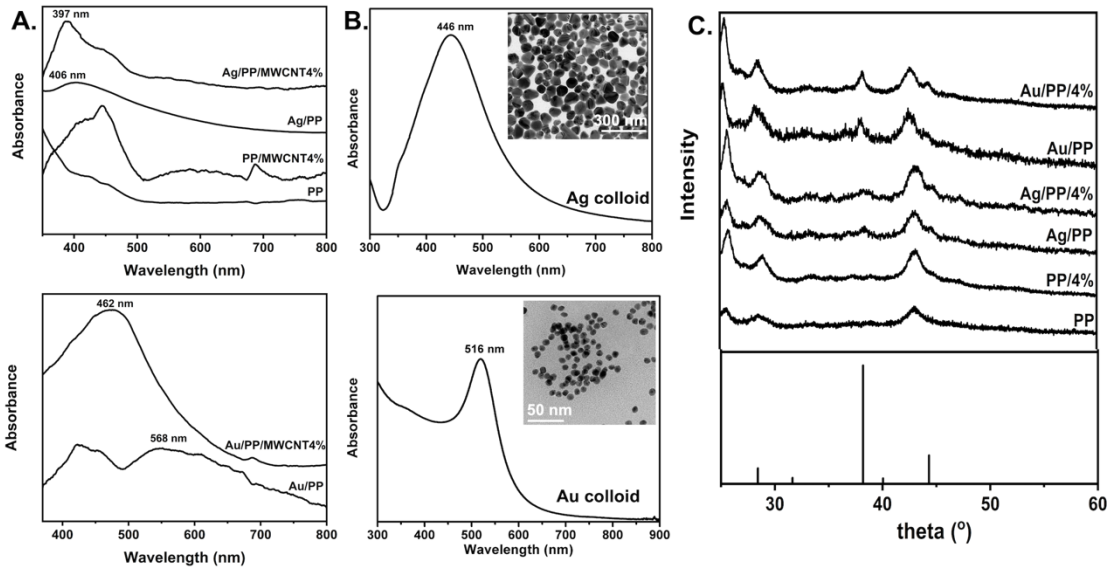

Figure S6: A. Visible absorption spectra (Kubelka–Munk converted reflectance spectra) of neat PP, PP4%, Ag/PP, Ag/PP4%, Au/PP and Au/PP4% filaments (left); Optical spectra of colloidal Ag NPs and Au NPs (right). Inset: TEM images of Ag and Au NPs. B. XRD diffractogram of PP, PP4%, Ag/PP, Ag/PP4%, Au/PP and Au/PP4% filaments and the reported reflexions for crystalline gold or silver with fcc structure (JCPDS Card No. 04-0784).

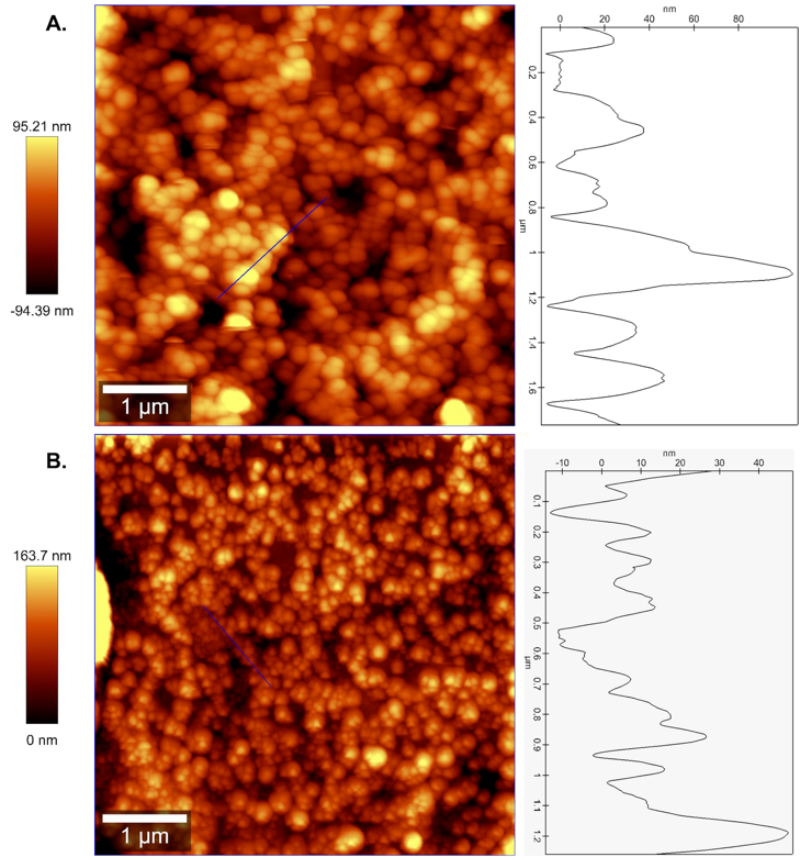

Figure S7: AFM topography images 5µm x 5µm (left) and topographic profile (marked by the blue line in the images) (right) of a) Ag/PP4% and b) Au/PP4%.

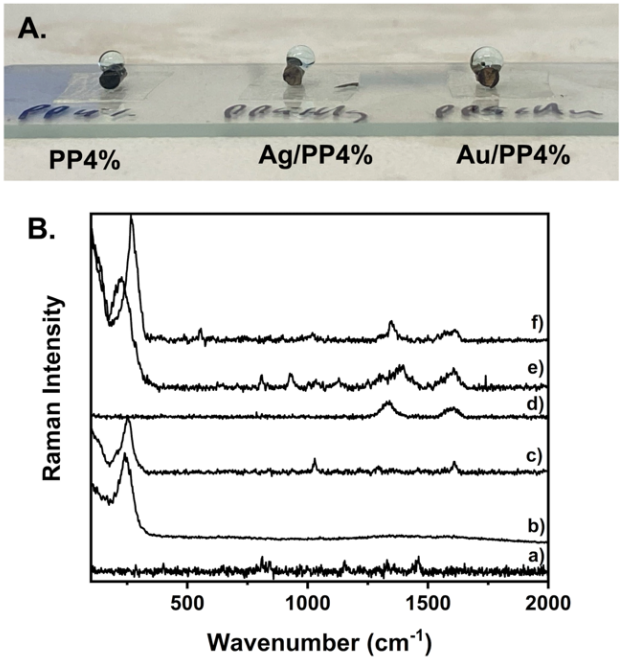

Figure S8: A. Digital photograph of MB droplets (100 µM, 10µL) deposited on the PP4% and metal NPs-loaded PP4%; B. Average of 10 Raman spectra of PP (a), Ag/PP (b), Au/PP (c), PP4% (d), Ag/PP4% (e) and Au/PP4% (f) using the 633nm excitation source (0.1mW, 2s 10aq).

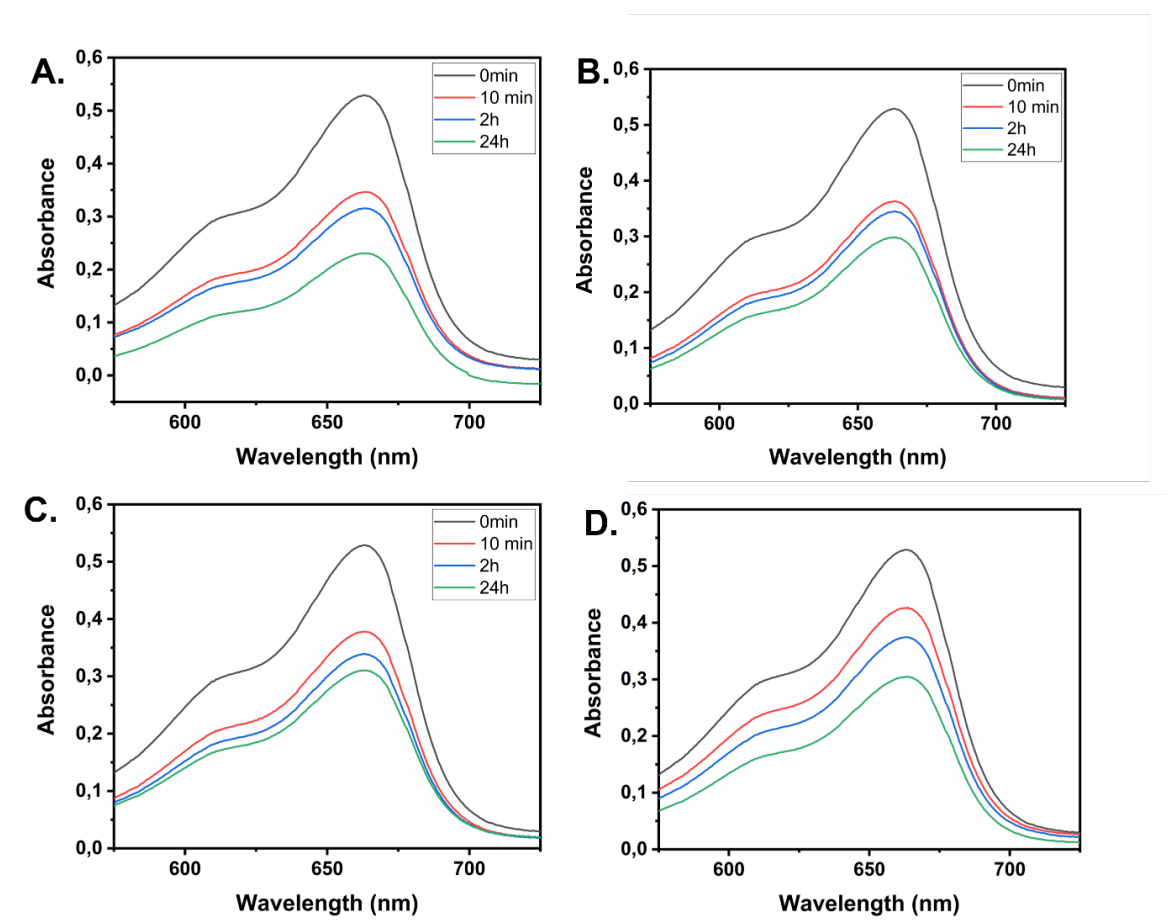

Figure S9: Time-dependent UV–Vis spectra of the MB (10 µM, 20ºC, pH 9) in the presence of the 3D_ Ag/PP4%cell (A); 3D_Ag/PP4%non (B), 3D_PP4%cell(C) and 3D_PPcell (D) structures.

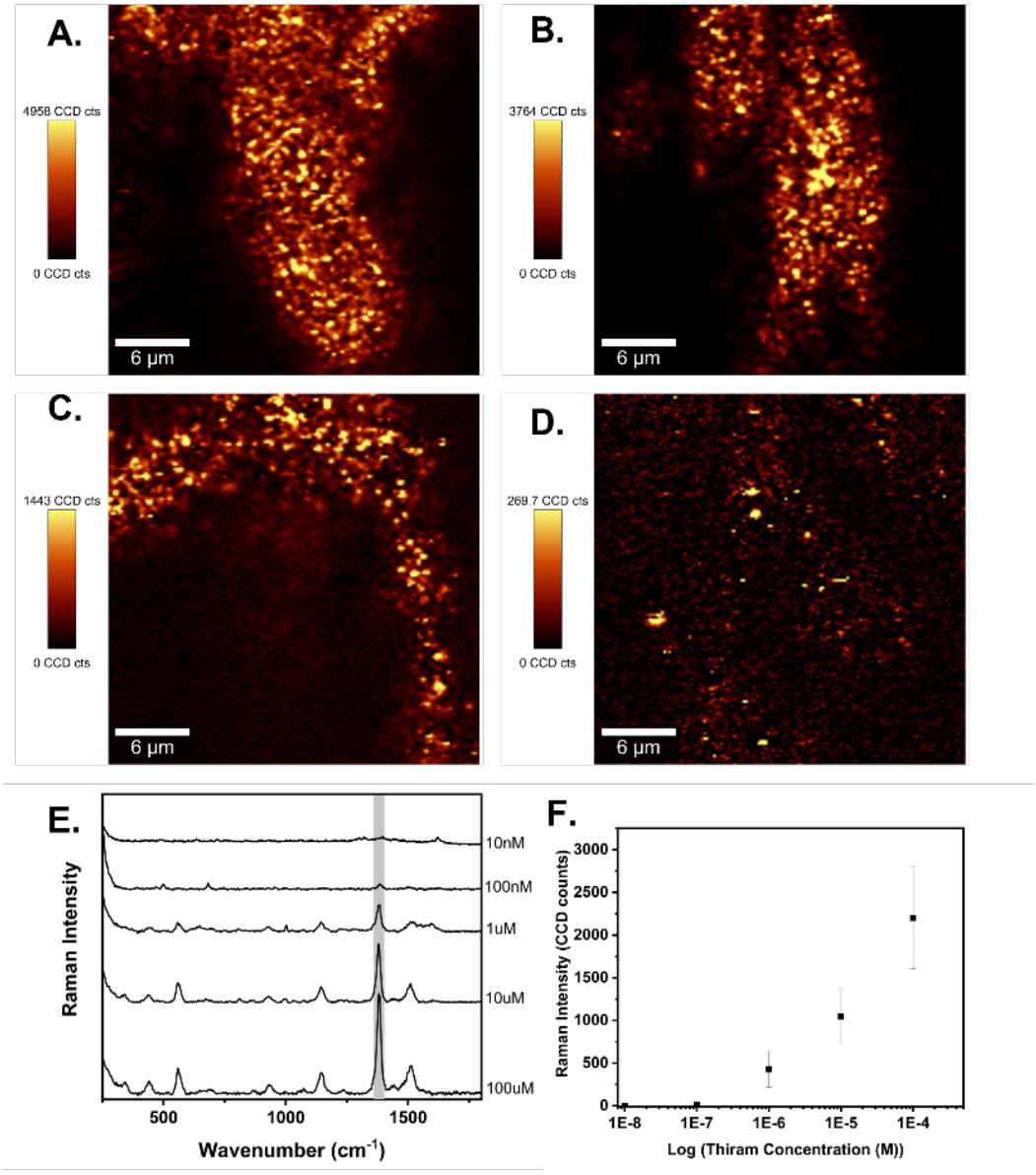

Figure S10: Raman images obtained with the integrated intensity of the band at 1380 cm^{-1} of thiram recorded using Ag/PP4% filament as SERS sensor for samples of thiram with variable concentrations: (A) 100 µM; (B) 10 µM; (C) 1 µM; (D) 100nM. The vertical bar shows the colour profile in each image, with the relative intensity scale. (E) Average of 10 SERS spectra of thiram taken from the Raman images in ultrapure water with variable thiram concentrations; (F) Intensity plot of the 1380 cm^{-1} thiram Raman band for varying thiram concentrations, using three different samples (Ag/PP4%) for each concentration.

Figure S11: Ag/PP4% test strip with a drop of paraquat 100 µM to be used as SERS sensors using a portable Raman spectrometer.

References

[1] E. Andreassen, in *Polypropylene*, Springer, Dordrecht, **1999**, pp. 320–328.
[2] X. Dong, H. Gu, J. Kang, X. Yuan, J. Wu, *Colloids Surf A Physicochem Eng Asp* **2010**, *368*, 142.
[3] G. N. Xiao, S. Q. Man, *Chem Phys Lett* **2007**, *447*, 305.
[4] S. Fateixa, M. Wilhelm, H. I. S. Nogueira, T. Trindade, *Journal of Raman Spectroscopy* **2016**, *47*, 1239.
[5] S. Fateixa, M. Raposo, H. I. S. Nogueira, T. Trindade, *Talanta* **2018**, *182*, 558.
[6] S. Sánchez-Cortés, C. Domingo, J. v. García-Ramos, J. A. Aznárez, *Langmuir* **2001**, *17*, 1157.
[7] S. Sánchez-Cortés, M. Vasina, O. Francioso, J. V. García-Ramos, *Vib Spectrosc* **1998**, *17*, 133.
[8] Y. Zhu, J. Wu, H. Gao, G. Liu, Z. Tian, J. Feng, L. Guo, J. Xie, *RSC Adv* **2016**, *6*, 59919.
[9] H. Fang, X. Zhang, S. J. Zhang, L. Liu, Y. M. Zhao, H. J. Xu, *Sens Actuators B Chem* **2015**, *213*, 452.
[10] M. Forster, R. B. Girling, R. E. Hester, *Journal of Raman Spectroscopy* **1982**, *12*, 36.